ARTICLE

doi:10.1016/S1525-0016(03)00122-9

Caveolae-Mediated Internalization of Extracellular HIV-1 Tat Fusion Proteins Visualized in Real Time

Aldo Ferrari,[1,†] Vittorio Pellegrini,[1] Caterina Arcangeli,[1] Antonio Fittipaldi,[1] Mauro Giacca,[1,2] and Fabio Beltram[1]

[1]*NEST-INFM and Scuola Normale Superiore, Piazza dei Cavalieri 7, I-56126 Pisa, Italy*
[2]*Molecular Medicine Laboratory, International Centre for Genetic Engineering and Biotechnology, Area Science Park, Padriciano 99, 34012 Trieste, Italy*

[†]*To whom correspondence and reprint requests should be addressed. Fax: +39 50 509417. E-mail: a.ferrari@sns.it.*

The Tat protein from HIV-1, when fused with heterologous proteins or peptides, can traverse cell membranes. This ability has generated great interest due to potential therapeutic applications. However, the relevant cellular pathway and its dynamics have not been elucidated yet. Here we unravel the intracellular fate of exogenously added Tat fused with green fluorescent protein (GFP) in live HeLa and CHO cells, from the early interaction with the plasma membrane up to the long-term accumulation in the perinuclear region. We demonstrate that the internalization process of full-length Tat and of heterologous proteins fused to the transduction domain of Tat exploits a caveolar-mediated pathway and is inhibited at 4°C. Remarkably, a slow linear movement toward the nucleus of individual GFP-tagged Tat-filled caveolae with an average velocity of 3 μm/h was observed. No fluorescence was observed in the nucleus, possibly suggesting that Tat fusion protein unfolding is required for nuclear translocation. In addition, early sensitivity to cytochalasin-D treatment indicates the essential role of the actin cytoskeleton in the displacement of Tat vesicles toward the nucleus. Our results imply that HIV-1 Tat mediates the internalization of protein cargos in a slow and temperature-dependent manner by exploiting the caveolar pathway.

Key Words: Tat, HIV-1, caveolae, GFP, protein transduction

INTRODUCTION

The Tat protein of human immunodeficiency virus type 1 (HIV-1) is an 86- to 101-amino-acid regulatory protein that transactivates HIV-1 provirus expression [1]. In addition, Tat can be released from productively infected cells [2,3]. This extracellular Tat can be then internalized into uninfected cells where it affects several cellular functions [4–8]. The ability of exogenous Tat to be taken up by cells has generated great interest owing to the potential therapeutic applications of this molecule. Tat, in fact, can be used as a vector for delivering heterogeneous proteins and drugs that would otherwise not have access to the intracellular environment [9]. Several studies have shown that different substances conjugated to Tat can in this way cross the cellular membrane [10]. Studies of several Tat-derived peptides demonstrated that residues 48 to 60 from the basic domain (the protein transduction domain or PTD) are responsible for the functional internalization into cells [11–13] and that cellular heparan sulfates (HS) act as low-affinity cellular receptors for the anchorage to the membrane [14,15]. Despite the amount of interest in these properties, the transduction mechanism by which Tat-functionalized molecules cross lipid bilayers and accumulate into the cells remains still largely unknown. Recent experimental studies, in addition, have even raised concerns about the efficacy of Tat-derived peptides to translocate across cellular membranes [16] and suggested that the uptake did not occur in a fast and temperature-independent way as previously believed [17].

Translocation processes of exogenous proteins and viral particles and visualization of their intracellular fates are challenging subjects of great current interest. Developments of high-resolution imaging techniques together with advanced molecular biology studies offer opportunities for these investigations with the potential of unraveling events not accessible by more conventional studies [18]. Recent work, for instance, demonstrated that some

1525-0016/03 $30.00

nonenveloped viruses like SV40 [19], polyomavirus [20], and echovirus 1 [21] can enter cells through a nonclassical, clathrin-independent endocytosis. An increasing body of evidence indicates that these internalization processes are regulated by a caveolar-mediated pathway. Caveolae are invaginated plasma membrane domains characterized by the presence of the integral membrane protein caveolin-1 (Cav-1). They are involved in many endogenous cellular processes like cholesterol homeostasis, glycosphingolipid transport, and glycosylphosphatidylinositol (GPI) anchored protein recycling [22]. There is also evidence that HIV-1 virus can use caveolae for transcytosis across the endothelium [23]. Among the other ligands or membrane elements that were found to internalize through this pathway are cholera toxin [24], folic acid, and the GPI–GFP fusion protein [25]. Specific cell-type differences were shown: while in CHO cells the process is rather fast and constitutive [26], in HeLa cells and in the absence of specific triggers, caveolae are largely immobile plasma membrane compartments not involved in constitutive endocytosis [27].

Green fluorescent proteins (GFPs) have emerged in the past years as powerful reporter molecules for the study of protein localization and trafficking within secretory and endocytic membranes of living cells [19,26–28]. In particular, GFPs have been used in a wide variety of applications aimed at defining the type of endocytic pathway utilized by various viruses [29]. GFP labeling has also been used to examine the morphological transformations occurring upon cell treatment with membrane traffic perturbants [12,18,26,27]. In the present work we exploited GFP tagging, high-resolution epifluorescence, and confocal imaging techniques to investigate the internalization kinetics of a Tat–enhanced green fluorescent protein (eGFP) fusion protein with glutathione *S*-transferase (GST-Tat-eGFP in the following) into living cells. Taking advantage of high sensitivity and depth of field of wide-field fluorescence microscopy we followed the cellular transduction in real time from the early interaction with the cell membrane up to the accumulation close to the cellular perinuclear region. The aim of our study was to elucidate the type of endocytic pathway utilized by Tat fusion proteins and determine the kinetics of the long-term vesicle movement within the cell, with the perspective of using Tat-mediated transduction for molecular therapy applications. Our results imply that GST-Tat-eGFP chimeras enter cells by a caveolar-mediated pathway and localize in the perinuclear region through actin-vehicled slow movements.

RESULTS

GST–Tat fusion proteins can enter cells when added exogenously [30,31] and this property was used to explore the mechanism of HIV-LTR transactivation by Tat. In particular, eGFP has proven to be a useful tag for the study of Tat transduction both in cultured cells and in specific tissue cells [32]. In addition, since its fluorescence can be detected only when the protein is correctly folded, the optical emission intensity can be used as a marker of intracellular pH changes [33]. Moreover, a GST-Tat-eGFP fusion protein maintains its ability to bypass cellular membranes and transactivate the HIV-LTR reaching a plateau at the concentration of 8 nM (0.5 μg/ml) [15].

Real-Time Visualization of GST-Tat-eGFP Entry in Live Cells

We added GST-Tat-eGFP fusion protein to HL3T1 cultured cells at concentrations ranging from 8 to 50 nM (from 0.5 to 3 μg/ml). The fluorescent signal from eGFP (indicating correctly folded protein) was visualized starting from a few minutes after the proteins were added (Fig. 1a) and was initially uniformly localized on the plasma membrane of the cells. Starting from 15 min after addition of the proteins at 37°C we observed the fluorescent signal in discrete vesicles on the plasma membrane. With laser irradiation at 488 nm, the fluorescent vesicles appeared as round-shaped fluorescent spots. At high concentration (50 nM) the signal from a single fluorescent vesicle increased, thereafter peaking at 90 min after protein addition (Fig. 1b). Detailed analysis of this fluorescence intensity after 90 min and comparison with photon counts obtained from single eGFPs [34] allowed us to estimate an average number of included fluorescent fusion proteins of around 300 assuming pH values not lower than 6 within the vesicles. We obtained similar results by adding GST-Tat-eGFP under similar conditions to CHO-K1 cell cultures (data not shown). Inclusion of the fluorescent signal into vesicles was prevented by incubating at 4°C. At this temperature and after protein addition, a weak and diffuse green fluorescent signal at the membrane was observed (see Fig. 1c). This signal was associated with Tat fusion proteins in close proximity to the cell membrane. Before adding the proteins, we observed no fluorescent signal distinct from the background at the cellular membrane with either lamp or laser illumination. Strong fluorescence emission from discrete vesicles could be readily recovered by raising the temperature of incubation back to 37°C (Figs. 1c and 1d). In agreement with previously reported data [15] we did not detect any association with cellular membranes or vesicle inclusion when cells were treated with heparin (Fig. 1e). CHO-K1 cells defective in HS biosynthesis also scored negative for membrane adhesion and fluorescent vesicle formation (Fig. 1f). Cells scored negative for membrane adhesion or vesicle inclusion of the fluorescent signal when a control GST–eGFP fusion protein was added in similar concentrations (data not shown).

Kinetics of GST-Tat-eGFP Vacuolar Trafficking

To explore GST-Tat-eGFP vacuolar trafficking from the plasma membrane into the interior of the cell, we performed

doi:10.1016/S1525-0016(03)00122-9

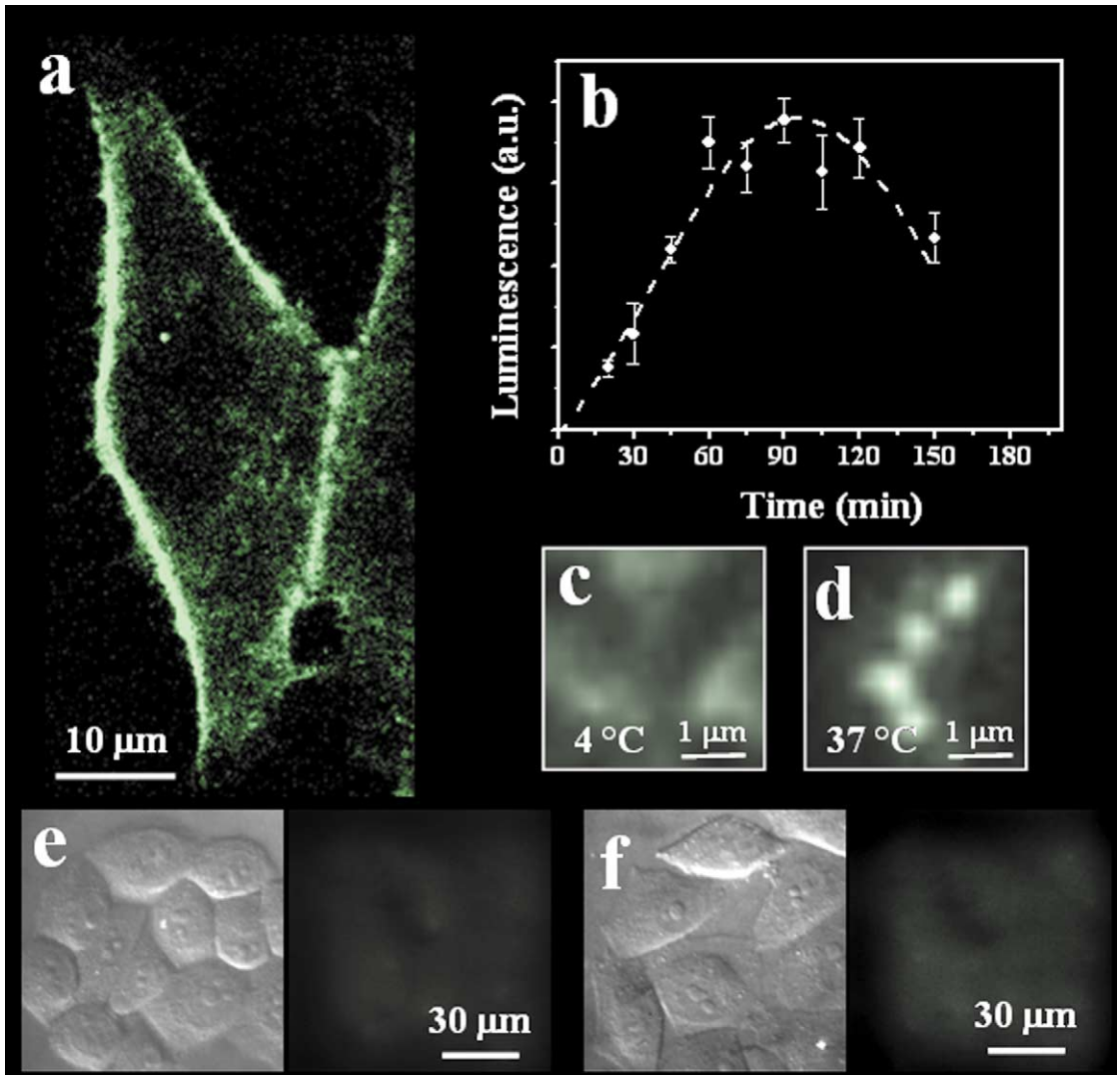

FIG. 1. Anchorage and vesicle inclusion of GST-Tat-eGFP fusion protein. (a) Laser-scanning confocal fluorescence image of live HL3T1 cells 90 min after GST-Tat-eGFP addition (50 nM) at 37°C. Fluorescence is distributed mainly on the plasma membrane. (b) Fluorescence of single GST-Tat-eGFP on the plasma membrane as a function of time after protein addition (50 nM) to HL3T1 cells. Fluorescence is expressed as arbitrary units, dots correspond to means, bars to standard errors of 10 individual vesicles and the white dotted curve is a guide to the eye; a peak of fluorescence at 90 min after protein addition is observed. (c and d) Wide-field fluorescence analysis of plasma membrane of live HL3T1 cells immediately after GST-Tat-eGFP anchorage (50 nM) at (c) 4°C and (d) 37°C; no fluorescence signal is observed at 4°C. (e) Wide-field fluorescence image of heparin-treated (1 μg/ml) HL3T1 cells after GST-Tat-eGFP addition (50 nM) and corresponding Nomarski image. (f) Wide-field fluorescence image of CHO-K1 mutants deficient in HS biosynthesis after GST-Tat-eGFP addition (50 nM) and corresponding Nomarski image.

live-cell time-lapse analysis to visualize individual eGFP-positive vesicles moving in the intracellular environment and defined their kinetics. No significant movement of eGFP-positive vesicles could be appreciated by fast dynamics analysis on HL3T1 cells (on the time scale of a few minutes), suggesting that those structures were highly stable when imaged in this time window (data not shown). By scanning a single confocal plane corresponding to the intracellular region of the cell, we saw that GST-Tat-eGFP-positive vesicles were initially confined to the periphery of the cell, drawing a ring close to the plasma membrane. They subsequently moved inward and reached the perinuclear region starting after 2.5 h (Fig. 2a). We performed long-term three-dimensional analysis of movements of individual GST-Tat-eGFP vesicles in HL3T1 cells up to 8 h after protein addition. eGFP fluorescence was excited each 15 min by an Hg lamp to minimize photobleaching and cell damage and collected by an intensified CCD camera. The reconstructed time-lapse

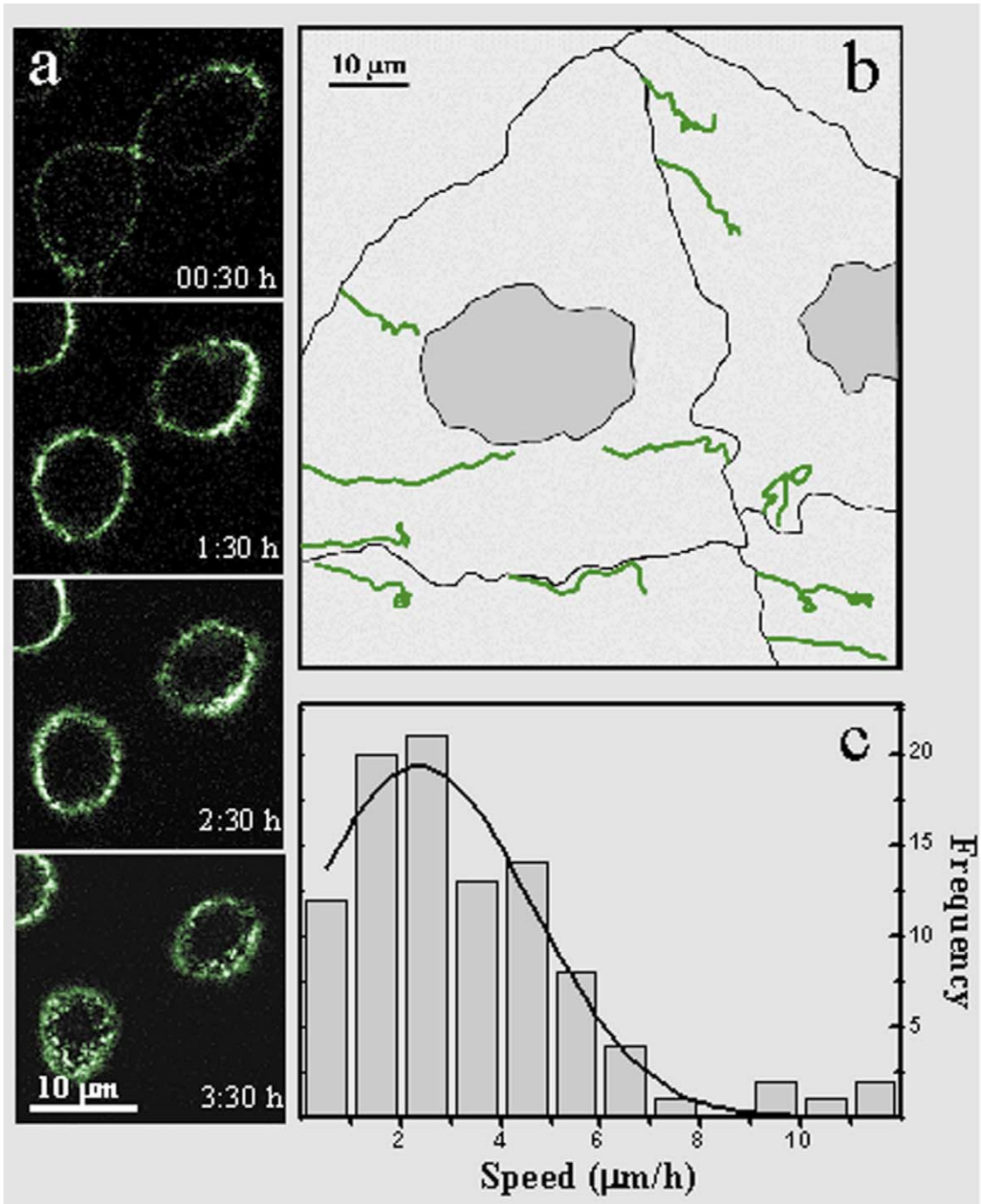

FIG. 2. Long-term tracking of individual GST-Tat-eGFP vesicles. Selected frames of a laser-scanning confocal fluorescence recording (z = 6 μm) at 37°C of HL3T1 cells after GST-Tat-eGFP addition (50 nM). (a) GST-Tat-eGFP vesicles move toward the nucleus. (b) Tracks of GST-Tat-eGFP vesicles (n = 11) whose trajectories were recorded every 15 min and followed up to 8 h at 37°C in HL3T1 cells by wide-field fluorescence microscopy; cells are shown in light gray and nuclei in dark gray . (c) Frequency of velocity measurements. The bar graph shows the number of measurements in a given velocity range (total number is n = 86) from 10 individual vesicles. The probability function (dark curve) was obtained by fitting data with a Gaussian distribution (α = 0.005, χ^2 = 4.27, r^2 = 0.94).

doi:10.1016/S1525-0016(03)00122-9

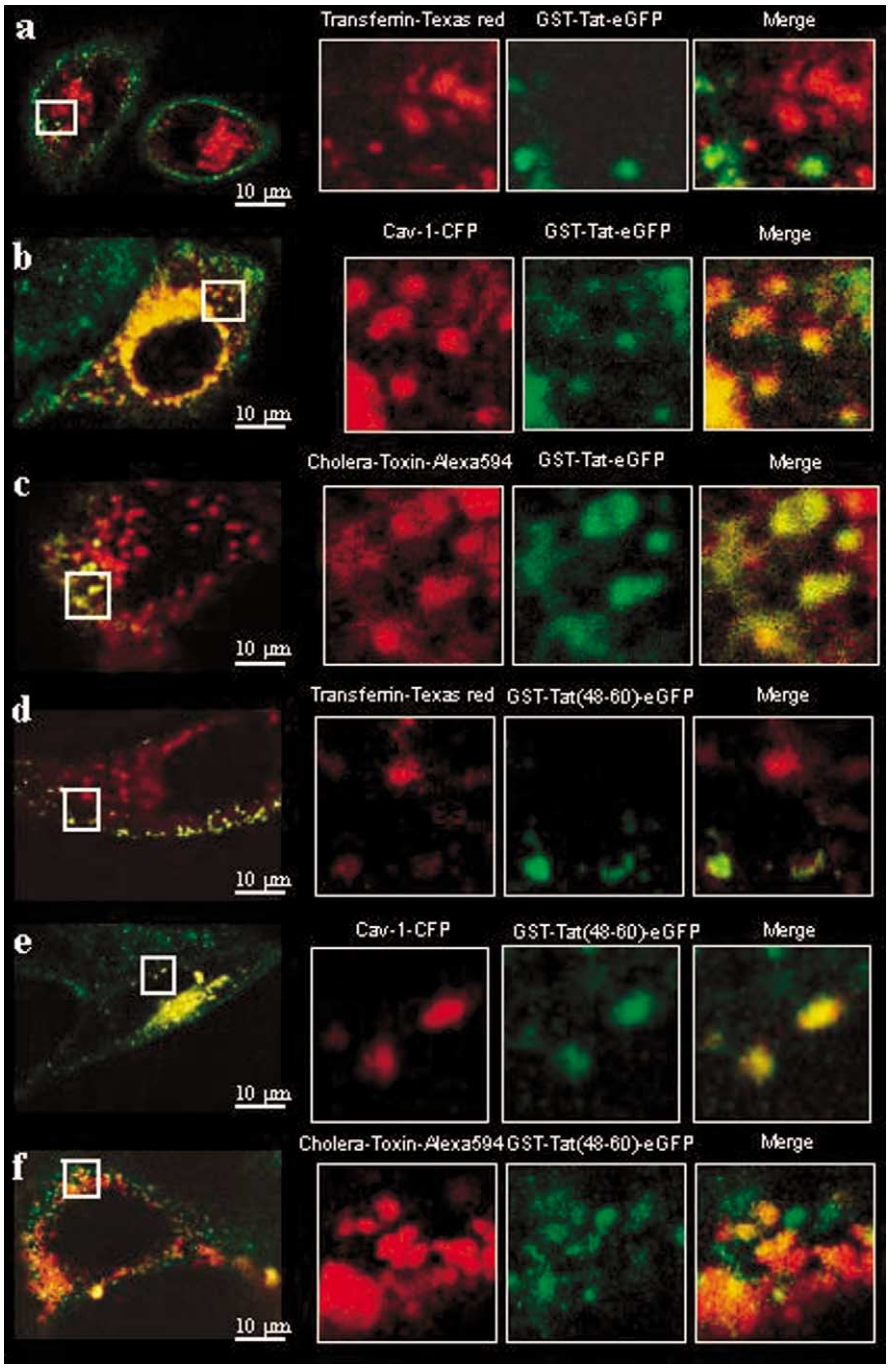

FIG. 3. GST-Tat-eGFP and GST-Tat(48-60)-eGFP vesicles colocalize with Cav-1. Laser-scanning confocal fluorescence images of live HL3T1 cells after transferrin-Texas red (50 μg/ml, red) and (a) GST-Tat-eGFP (50 nM, 3 μg/ml, green) or (d) GST-Tat(48-60)-eGFP (54 nM, 3 μg/ml, green) addition at 37°C. Laser-scanning confocal live fluorescence images of Cav-1-CFP (red)-transfected HL3T1 cells after (b) GST-Tat-eGFP (50 nM, 3 μg/ml, green) or (e) GST-Tat(48-60)-eGFP (54 nM, 3 μg/ml, green) addition at 37°C; CFP fluorescence is depicted in red for better visualization. Laser-scanning confocal live fluorescence images of HL3T1 cells after cholera toxin-Alexa 594 (10 μg/ml, red) and (c) GST-Tat-eGFP (50 nM, 3 μg/ml, green) or (f) GST-Tat(48-60)-eGFP (54 nM, 3 μg/ml, green) addition at 37°C.

FIG. 4. GST-Tat-eGFP accumulation in Cav-1 perinuclear structures. Three-dimensional reconstruction of a confocal *z* scansion (34 steps of 0.3 μm each) of the colocalization signal between GST Tat-eGFP (green) and Cav-1-CFP (red) in a positively transfected HL3T1 cell 3 h after protein addition. On the back the same scansion is depicted as a two-dimensional maximum projection.

FIG. 5. Effects of cytochalasin-D and nocodazole. Maximum projections of laser-scanning confocal fluorescence *z* recording (0.3-μm step) after addition of GST-Tat-eGFP (50 nM, 3 μg/ml, green) together with transferrin-Texas red (50 μg/ml, red) to (a) cytochalasin-D-treated (5 μM), (c) untreated, and (e) nocodazole-treated (20 μM) HL3T1 cells. Vector tracks of typical GST-Tat-eGFP vesicle trajectories (recorded every 15 min and followed up to 8 h at 37°C by wide-field fluorescence microscopy) observed in (b) cytochalasin-D-treated (5 μM), (d) untreated, and (f) nocodazole-treated (20 μM) HL3T1 cells.

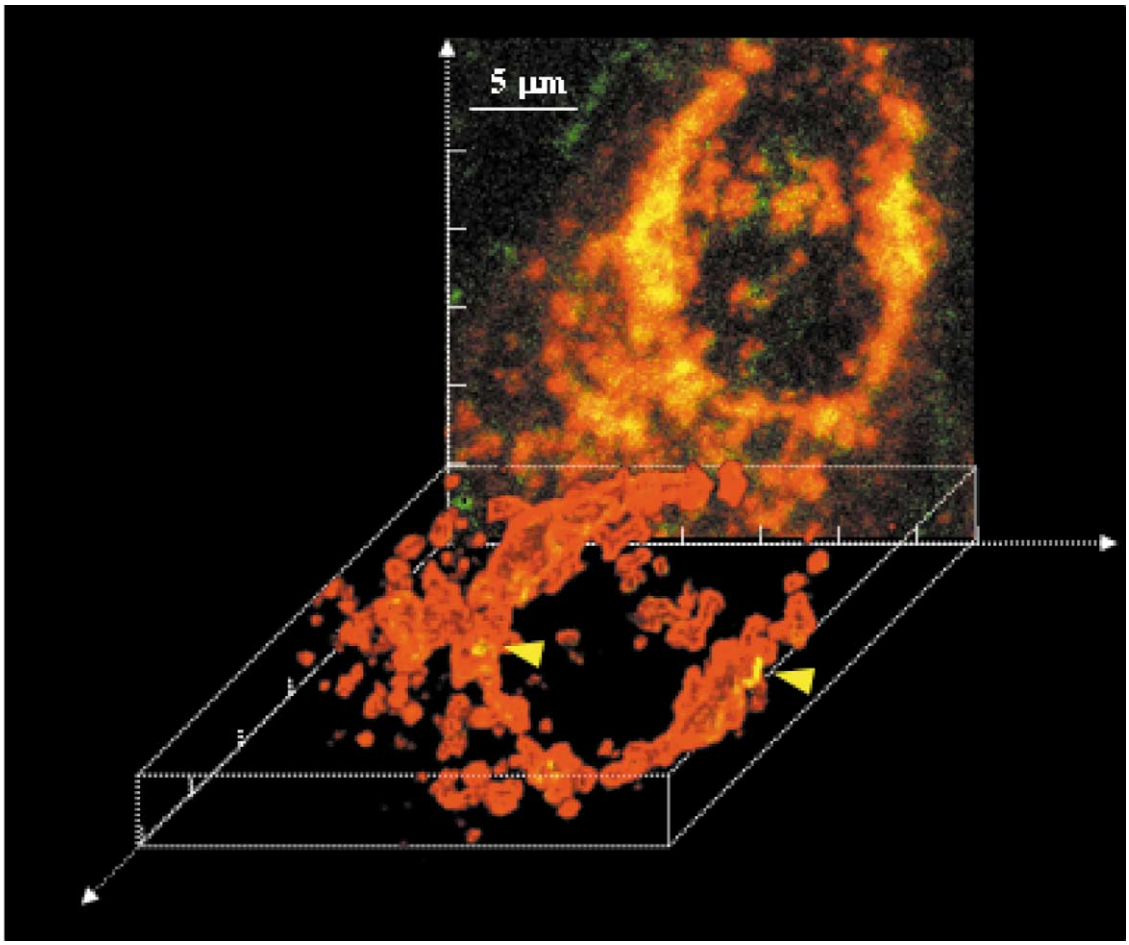

4

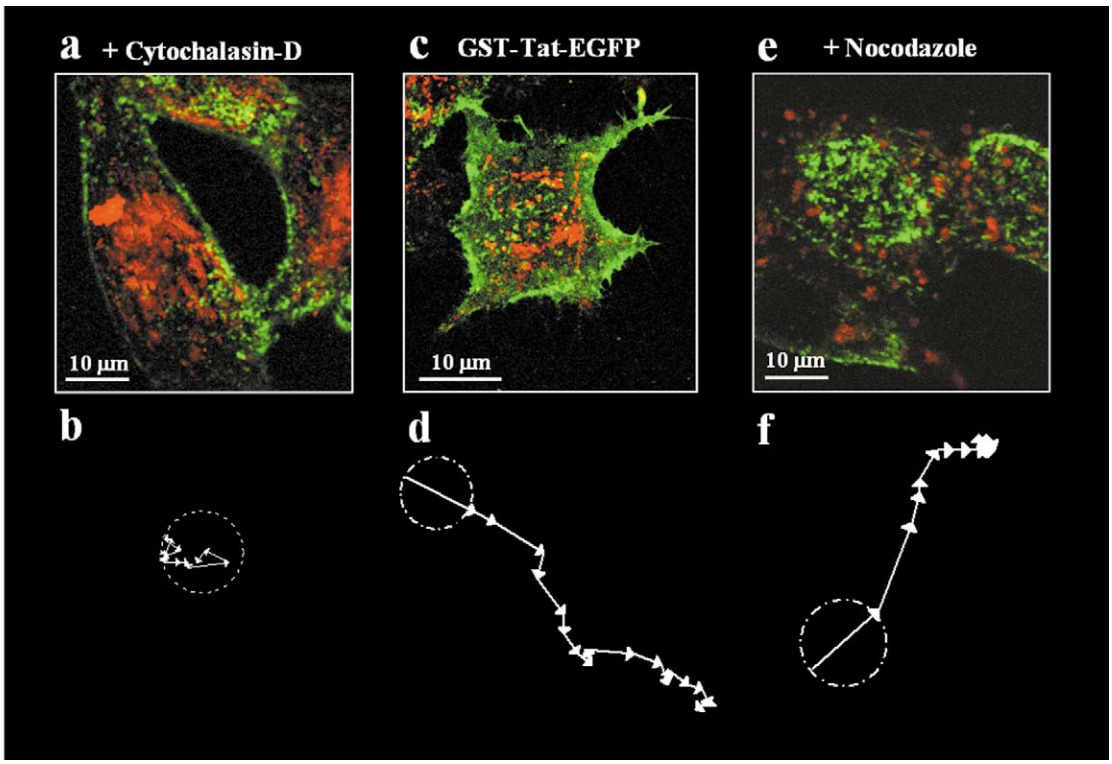

5

doi:10.1016/S1525-0016(03)00122-9

allowed us to draw the tracks of individual eGFP-positive vesicles (Fig. 2b). Most of the tracked vesicles move directly toward the nucleus while a few of them remain localized in a region close to the plasma membrane. The statistical analysis of individual vesicle velocity yields a Gaussian-like distribution (Fig. 2c) with a peak around 3 μm/h and a small shoulder at approximately 12 μm/h.

GST-Tat-eGFP is Selectively Recruited in Caveolar Structures

To obtain direct visual evidence of the association between a specific endocytic pathway and the GST-Tat-eGFP vesicular internalization described above, we performed live-cell colocalization experiments with transferrin-Texas red, a positive marker of clathrin-mediated endocytosis, and a C-terminally cyan fluorescent protein (CFP)-tagged caveolin-1 (Cav-1-CFP) fusion protein, a marker for caveolar endocytosis, on both HL3T1 and CHO-K1 cells. When added together with GST-Tat-eGFP, transferrin-Texas red showed a faster accumulation in the cytosol. We measured the average velocity for transferrin-Texas red-positive endosomes in live-cell time-lapse confocal analysis at around 0.5 μm/s. This velocity is compatible with previous results on transferrin-Texas red-positive endosomes [35] but is three orders of magnitude faster than the velocity recorded for GST-Tat-eGFP-positive vesicles. These transferrin-Texas red-positive endosomes, in addition, did not colocalize with GST-Tat-eGFP-positive vesicles to a significant extent (Fig. 3a). No colocalization could be observed up to 8 h after protein addition. To visualize the caveolar internalization pathway we transfected cells with a plasmid encoding Cav-1-CFP. It has been previously shown that Cav-1-fluorescent protein chimeras are reliable markers for endogenous Cav-1 in CHO cells [26] and are correctly sorted to caveolae at the plasma membrane in HeLa cells [27]. Moreover they do not affect the normal activity of the caveolar internalization pathway [19]. In our experiments we found a significant colocalization signal between GST-Tat-eGFP and Cav-1-CFP starting from approximately 1 h after protein addition to the cell culture and increasing thereafter (Fig. 3b). A strong colocalization signal was indeed observed at later times when GST-Tat-eGFP was found to localize in the perinuclear region. We obtained similar results when colocalization experiments on live cells were performed after adding GST-Tat(48-60)-eGFP instead of the full-length GST-Tat-eGFP fusion protein. No significant colocalization could be observed between GST-Tat(48-60)-eGFP and transferrin-Texas red up to 8 h after protein addition (Fig. 3d), whereas a strong colocalization between GST-Tat(48-60)-eGFP and Cav-1-CFP in positively transfected cells was appreciable with the same kinetics displayed by the full-length GST-Tat-eGFP fusion protein (Fig. 3e). We found similar colocalization results in CHO-K1 cells (data not shown). To confirm GST-Tat-eGFP and GST-Tat(48-60)-eGFP inclusion in caveolar vesicles and to rule out the effect of Cav-1-CFP overexpression in transiently transfected cells we also performed live-cell colocalization with cholera toxin-Alexa 594, which exploits the caveolar pathway to enter cells [24]. Also in this case we found a significant colocalization (Figs. 3c and 3f). After 2–4 h from GST-Tat-eGFP addition, the fluorescent signal was observed, in most of the cells, in tube-shaped Cav-1-positive organelles localized in the perinuclear region of the cells, most probably corresponding to the caveosome structure [19]. Fig. 4 shows the three-dimensional reconstruction of the colocalization signal of a HL3T1 cell expressing Cav-1-CFP (a confocal colocalization image is also shown in Fig. 4) 4 h after addition of Tat fusion proteins. Here the caveosome appears as a largely interconnected perinuclear network of irregularly shaped tubular structures, some of which contain GST-Tat-eGFP in their cavities (indicated by arrows in Fig. 4).

Effects of Cytochalasin-D and Nocodazole Treatment on GST-Tat-eGFP Internalization

To demonstrate further that internalization of Tat fusion proteins exploits the caveolar endocytic system, we tested the effects of drugs that selectively disrupt either cell microfilaments or microtubules. After drug treatment GST-Tat-eGFP was added together with transferrin-Texas red. It is known that treatment with cytochalasin-D yields a depolymerization of the actin cytoskeleton that forces the caveolae still connected to the cellular surface to move laterally and to cluster on the plasma membrane [36,37]. Fig. 5a shows the maximum projection of a *z* scansion of a cytochalasin-D treated cell 8 h after addition of the protein. In the presence of both GST-Tat-eGFP and transferrin-Texas red the majority of GST-Tat-eGFP-positive caveolae are still connected to the surface compared to a drug-free control (Fig. 5c), while transferrin-Texas red was correctly displaced into the intracellular environment. The latter observation rules out any possible toxic effect causing a general impairment of the cellular endocytic pathways. Wide-field microscopy tracking of individual GST-Tat-eGFP caveolae in cytochalasin-D-treated cells up to 8 h after addition of the protein (Fig. 5b) showed a typical behavior characterized by limited random movements in a restricted area of the plasma membrane.

In contrast, treatment of cells with nocodazole caused microtubule disruption as confirmed by transferrin-Texas red localization 8 h after addition of the proteins (Fig. 5e), while GST-Tat-eGFP fluorescence appeared mostly localized in the perinuclear region. Tracks of individual GST-Tat-eGFP caveolae (Fig. 5f) in nocodazole treated cells indicated direct movement toward the inner part of the

cell similar to that visualized in drug-free control experiments (Fig. 5d).

DISCUSSION

Frankel and Pabo [38] first demonstrated the ability of HIV-1 Tat protein to enter cells, localize in the nucleus, and transactivate the HIV-1 promoter when added to the cell culture medium. Internalization was observed in the absence of specific receptors and this raised the possibility of using Tat as a vector able to deliver selected biomolecules into the cells. Following this work, extensive molecular analysis of Tat proteins identified a short arginine-rich domain (Tat 48-60), called Tat-PTD, responsible for the transduction process across cellular membranes [11]. The potential of this domain as cargo vector has been already exploited in different cell types [13]. Despite an intense research effort, the mechanism of transduction responsible for the entry of full-length Tat and Tat-PTD into cells is still poorly understood. In a pioneering work, however, Mann and Frankel [39] ascribed the cellular uptake of exogenously added Tat protein to an energy-dependent endocytosis pathway. One of the limitations of most of the available studies on Tat delivery is that they are based on imaging experiments on fixed cells [40].

Motivated by these considerations, here we provide a complete dynamics analysis of the transduction mechanism of full-length Tat and Tat-PTD fusion proteins, from the early interaction with the cell membrane up to the long-term trafficking in the cytosol. All data were taken on live HeLa-HL3T1 and CHO-K1 cells.

The main experimental findings can be summarized in the following three points: (i) exogenous GST-Tat-eGFP fusion proteins rapidly bind to the cellular membrane in a temperature-independent way. Early anchorage, however, is followed by inclusion of the fluorescent signal into round-shaped vesicles through a temperature-dependent process. The inclusion process proceeds, reaching a peak of included protein concentration 2 h after protein addition. The following drop (see Fig. 1) can be explained by a progressive decrease in extracellular concentration of free proteins in the culture medium. (ii) Long-term tracking of GST-Tat-eGFP-positive vesicles shows a very slow centripetal movement with an average velocity of about 3 μm/h. This slow movement is incompatible with the fast dynamics described for constitutive endocytic trafficking of clathrin-coated pits and vesicles [35]. Slow dynamics associated with an endocytic pathway was recently reported by Thomsen and co-workers [27]. In their work they demonstrated the existence of a nonconstitutive and highly stable Cav-1-positive endocytic pathway in transfected HeLa cells. The reported diffusion coefficient for caveolae is consistent with the average speed here observed for the case of GST-Tat-eGFP vesicles. This raised the possibility that internalization of Tat might exploit the caveolar system. (iii) The colocalization experiments shown in Fig. 3 clearly indicate that GST-Tat-eGFP chimeras follow a caveolar pathway and not the fast clathrin-dependent pathway. The same property is shared by a GST-Tat(48-60)-eGFP fusion protein.

Several nonenveloped viruses and some bacterial toxins together with membrane constituents and other ligands use the caveolar pathway to enter cells [41]. This mechanism provides a nonacidic, nondigestive route for cellular internalization. This nonclassical pathway has been extensively studied for SV40 [42]. In this case, it was demonstrated that the inclusion of the SV40 particle in the caveolae triggers phosphorylation of tyrosine residues in proteins associated with the caveolae. Indeed only virus-loaded caveolae were found to detach from the membrane plane within 3 min [19]. In our observations neither GST-Tat-eGFP nor GST-Tat(48-60)-eGFP was able to modify the dynamics of Cav-1-positive vesicles, and the rate of membrane-bound caveolae detachment was comparable to that of control cells when no protein was added. We thus conclude that Tat fusion proteins are internalized through a very slow but constitutive internalization process involving caveolar movement, which is observable only in the time window of a few hours. Additional evidences for this mechanism can be found elsewhere [43]. However, not all cell types exhibit the very slow caveolar dynamics described for HeLa cells. In CHO cells, for example, caveolae are internalized constitutively with a faster dynamics [26]. Consistently GST-Tat-eGFP and GST-Tat(48-60)-eGFP fusion proteins were found to be internalized in a faster, constitutive way when added under the same conditions to CHO-K1 cells (data not shown). In CHO-K1 cells the observed average velocity of GST-Tat-eGFP- and GST-Tat(48-60)-eGFP-positive vesicles was found to peak at 1.2 μm/min with maximum values up to 7–8 μm/min.

Cellular HS act as low-affinity and large-capacity receptors for GST-Tat-eGFP early anchorage (Fig. 1f and Ref. [15]) and heparin can prevent this interaction when added to the cell culture medium together with our fusion protein (Fig. 1e and Ref. [14]). It is thus conceivable that full-length Tat and Tat-PTD fusion proteins enter this pathway through membrane binding with HS, the latter being passively driven until the caveosome. This view is further supported by recent biochemical studies showing that cellular HS side chains in glypican-1, a member of the GPI-linked cell surface proteoglycan (PG) family, enter a recycling pathway through Cav-1-positive vesicles and perinuclear structures [44]. The enhanced transduction extended by the highly basic Tat-PTD can be explained in terms of faster and more efficient anchorage and inclusion into the caveolar pathway as suggested by Leifert and co-workers [16]. From this perspective, cell-type differ-

doi:10.1016/S1525-0016(03)00122-9

ences in the caveolae internalization rate must be taken into account when evaluating the efficiency of transduction of full-length Tat and Tat-PTD fusion proteins.

Additionally, it is interesting to note that internalization of a ligand along with this PG can redirect the products of HS degradation from caveolar structures to the nucleus [45]. The time course of GST-Tat-eGFP-mediated LTR-CAT transactivation was measured by some of us [15] on HL3T1 cells. Those results are compatible with the slow internalization dynamics of GST-Tat-eGFP caveolae here reported. This would imply a further displacement of full-length Tat and Tat(48-60) complexes from caveosome or caveolae to the nucleus. Moreover, Eguchi and co-workers [46] recently reported that inhibitors of caveolae formation can reduce by 50% the efficiency of a Tat-PTD phage-mediated gene transfer, strongly supporting an involvement of the caveolar pathway in the nuclear translocation of Tat-PTD complexes. To investigate nuclear translocation processes, the analysis of GST-Tat-eGFP nuclear accumulation would be required. We were not able, however, to localize the fluorescence of GST-Tat-eGFP or GST-Tat(48-60)-eGFP outside Cav-1-positive cytoplasmic structures nor in the nucleus up to 24 h after protein addition. A loss of eGFP fluorescence due to local acidification can be ruled out within the caveolar system, in which the pH values are maintained around neutrality [19]. Additionally, trafficking from the caveolar system to the Golgi complex has been followed for a GPI–GFP fusion protein without any detectable loss in fluorescence [25]. Bonifaci and co-workers [47] have demonstrated that an unfolding step is necessary for nuclear translocation of a full-length Tat fusion protein. Thus the most plausible explanation for eGFP fluorescence loss is that the unfolding step necessary for Tat-fusion protein nuclear translocation occurs during protein import into the nucleus or in some intermediate membrane system.

The actin cytoskeleton acts in stabilizing membrane-bound caveolar invaginations and might be responsible for their typical steady-state reduced diffusion coefficient [26,27,41]. Fig. 5 shows that while no remarkable changes are obtained by treating the cells with nocodazole, disruption of the actin filaments with cytochalasin-D results in an improved random movement on the plasma membrane of GST-Tat-eGFP-enriched caveolae. This observation reproduces what was already observed for SV40: initial transport to the caveosome is microtubule independent and relies on an intact actin network, while microtubule integrity could be necessary for the following steps. Nuclear transactivation experiments in nocodazole- and cytochalasin-D-treated cells should allow the clarification of the role of cellular cytoskeleton and the functional relevance of full-length Tat and Tat-PTD fusion protein caveolar internalization.

In conclusion, the present work indicates that full-length and Tat-PTD fusion proteins take advantage of the cellular caveolar system to exploit their transduction activity. In addition to the notion that many microbial pathogens exploit caveolar endocytosis as an entry route to infect cells, there is growing evidence that this pathway is involved in the pathogenesis of several human diseases, including cancer [48]. From the therapeutic point of view, in contrast, the observation here reported raises the additional possibility of exploiting Tat-derived peptides in molecular therapy protocols aimed at delivering specific drugs within the caveolar system of the cell.

MATERIALS AND METHODS

Cell lines. HL3T1 cells (HeLa derivative containing an integrated HIV-1 LTR driving the expression of a CAT reporter gene) were a kind gift from G. Pavlakis (National Cancer Institute, Fredericks Cancer Research Facility, Fredericks, MD). CHO-K1 and CHO-K1 mutants deficient in HS biosynthesis were obtained from the American Type Culture Collection (Manassas, VA). HL3T1 cells were cultured in Dulbecco's modified Eagle's medium with GlutaMax (Life Technologies, Inc., Invitrogen Corp., Carlsbad, CA). CHO cells were cultured in Ham's F10 medium with GlutaMax (Life Technologies, Inc.). Both media were supplemented with 10% fetal bovine serum (Life Technologies, Inc.) and gentamicin 100 μg/ml and were buffered with 20 mM Hepes. Cells were cultured at 37°C in a humidified 95% air, 5% CO_2 incubator.

Recombinant proteins. The plasmid expressing GST-Tat-eGFP was obtained by cloning a polymerase chain reaction-amplified fragment into the *Bam*HI and *Eco*RI sites of the commercial vector pGEX2T (Amersham Biosciences Corp., Piscataway, NJ). The fragment was obtained by the separate amplification of HXB2 Tat using primers 5′-GTGGATCCATGGAGCCAGTAGATCCTA-3′ and 5′-CCCTTGCTCACCATAAGCTTTTCCTTCGGGCC-3′ and of eGFP using primers 5′-GGCCCGAAGGAAAAGCTTATGGTGAGCAAGGG-3′ and 5′-GGCGACCTAGAGTCGCGGCCGCTTTA-3′. Templates for amplification were plasmid pGEX2T-Tat [30] and peGFP-N1 (Clontech, Palo Alto, CA), respectively. The two amplification products contain complementary sequences at the 3′ and 5′ ends of the coding strands of Tat and eGFP, respectively. They were gel purified, mixed, annealed, and amplified with the external primers to obtain single amplification products that contain *Bam*HI and *Eco*RI sites at the extremities. The plasmid expressing Cav-1-CFP fusion protein was a kind gift from L. Pelkmans (Institute of Biochemistry, Swiss Federal Institute of Technology, Zurich, Switzerland).

GST-Tat-eGFP protein transduction. To study the kinetics of recombinant GST-Tat-eGFP internalization, HL3T1 cells were seeded in 3- or 6-cm-diameter glass-bottom petri dishes at a density of 5–10 × 10^3 cells/cm^2 in Dulbecco's modified Eagle's medium containing 10% fetal calf serum. After an additional incubation for 30 min in serum-free medium, fresh medium containing GST-Tat-eGFP recombinant protein in various concentrations ranging from 8 to 50 nM was added. For live-cell recording the dishes were placed in a humidified Plexiglas chamber and maintained at 37°C and 5% CO_2 throughout each experiment. For the fast dynamics recording and colocalization experiments cells were imaged using a TCS-SP laser scanning confocal microscope (Leica Microsystems, Mannheim, Germany) with a 63×, 1.4 NA plan apochromatic lens using a computer-controlled 488 nm argon laser to excite eGFP, a 446 nm argon laser to excite CFP, and a 568 nm krypton laser to excite Texas red.

Long-term live-cell recording. For long-term visualization of GST-Tat-eGFP transduction the dishes were placed under an epifluorescence Axioskop-2 microscope (Zeiss, Carl Zeiss, Jena, Germany) with a 100×, 1.3 NA plan neofluar objective and Nomarski optics. eGFP fluorescence was excited with a 100-W HBO lamp and collected with a PentaMax 512-EFT intensified CCD camera (Princeton Instruments, Trenton, NJ) with detection time of 0.1 s, using the band-pass 450–490 excitation filter and the band-pass 515–565 emission filter of the Zeiss eGFP filter set.

Colocalization experiments. For the colocalization experiments eGFP and CFP were excited by 488 and 458 nm argon laser, respectively. Alexa 594 and Texas red fluorescence were excited by 543 nm krypton laser. To avoid cross talk occurring between GST-Tat-eGFP or GST-Tat(48-60)-eGFP and Cav-1-CFP, whose emission spectra are not sufficiently separated, we collected their emission signals independently in the 460–490 and 492–590 nm wavelength ranges, respectively. Emission signals from Texas red and Alexa 594 were collected in the 580–667 nm range. Colocalization was calculated by measuring the magnitude of Cav-1-CFP, cholera toxin-Alexa 594 or transferrin-Texas red signal overlaps with either GST-Tat-eGFP or GST-Tat(48-60)-eGFP signal using the "measure colocalization" function of MetaMorph Analysis v 4.5 (Universal Imaging Corp., West Chester, PA).

Experiments with cytochalasin and nocodazole. For the analysis of GST-Tat-eGFP transduction sensitivity to drugs, cell dishes were pretreated with serum-free fresh medium containing either 5 μM cytochalasin-D or 20 μM nocodazole (Sigma–Aldrich Corp., St. Louis, MO) for 30 min. Thereafter GST-Tat-eGFP and transferrin-Texas red were added as described above.

Data analysis. All fluorescence images acquired in wide-field microscopy were deconvoluted using the blind-deconvolution algorithm of AutoDeblur v 7.0 software (AutoQuant Imaging, Inc., Watervliet, New York, NY). Tracking of individual GST-Tat-eGFP- and GST-Tat(48-60)-eGFP-positive caveolae was performed using MetaMorph and plotted with Origin Pro v 7.03 (OriginLab Corp., Northampton, MA). Three-dimensional reconstructions of *z* scansions acquired with the confocal setup were performed using the 3D-reconstruction function of Auto Visualize-3D v 5.1 (AutoQuant Imaging, Inc.).

ACKNOWLEDGMENTS

We acknowledge Paolo Faraci and Arianna Sabò (NEST-INFM and Scuola Normale Superiore) for technical assistance, and George Pavlakis (National Cancer Institute, Frederick Cancer Research Facility, Frederick, MD) for useful discussions. This work was supported by grants from MIUR and INFM.

RECEIVED FOR PUBLICATION FEBRUARY 11, 2003; ACCEPTED MARCH 19, 2003.

REFERENCES

1. Dingwall, C., *et al.* (1989). Human immunodeficiency virus 1 Tat protein binds trans-activation-responsive region (TAR) in vitro. *Proc. Natl. Acad. Sci. USA* **86:** 6925–6929.
2. Ensoli, B., Barillari, G., and Salahuddin, S. (1990). Tat protein of HIV-1 stimulates growth of cells derived from Kaposi's sarcoma lesions of AIDS patients. *Nature* **345:** 84–86.
3. Ensoli, B., *et al.* (1992). Release, uptake, and effects of extracellular human immunodeficiency virus type 1 Tat protein on cell growth and viral transactivation. *J. Virol.* **67:** 277–287.
4. Barillari, G., Gendelman, R., Gallo, R., and Ensoli, B. (1993). The Tat protein of human immunodeficiency virus type 1, a growth factor for AIDS Kaposi sarcoma and cytokine-activated vascular cells, induces adhesion of the same cell types by using integrin receptors recognizing the RGD amino acid sequence. *Proc. Natl. Acad. Sci. USA* **90:** 7941–7945.
5. Flores, S. C., *et al.* (1993). Tat protein of human immunodeficiency virus type 1 represses expression of manganese superoxide dismutase in HeLa cells. *Proc. Natl. Acad. Sci. USA* **90:** 7632–7636.
6. Howcroft, T. K., Strebel, K., Martin, M. A., and Singer, D. S. (1993). Repression of MHC class I gene promoter activity by two-exon Tat of HIV. *Science* **260:** 1320–1322.
7. Taylor, J. P., *et al.* (1992). Activation of expression of genes coding for extracellular matrix proteins in Tat-producing glioblastoma cells. *Proc. Natl. Acad. Sci. USA* **89:** 9617–9621.
8. Westendorp, M., Li-Weber, M., Frank, R. W., and Krammer, P. H. (1994). Human immunodeficiency virus type 1 Tat upregulates interleukin 2 secretion in activated T cells. *J. Virol.* **68:** 4177–4185.
9. Fawell, S., *et al.* (1994). Tat-mediated delivery of heterologous proteins into cells. *Proc. Natl. Acad. Sci. USA* **91:** 664–668.
10. Schwarze, S. R., and Dowdy, S. F. (2000). In vivo protein transduction: intracellular delivery of biologically active proteins, compounds and DNA. *Trends Pharmacol. Sci.* **21:** 45–48.
11. Vivès, E., Brodin, P., and Lebleu, B. (1997). A truncated HIV-1 Tat protein basic domain rapidly translocates through the plasma membrane and accumulates in the cell nucleus. *J. Biol. Chem.* **272:** 16010–16017.
12. Futaki, S., *et al.* (2001). Arginine-rich peptides. An abundant source of membrane-permeable peptides having potential as carriers for intracellular protein delivery. *J. Biol. Chem.* **276:** 5836–5840.
13. Schwarze, S. R., Hurska, K. A., and Dowdy, S. F. (2000). Protein transduction: unrestricted delivery into all cells. *Trends Cell Biol.* **10:** 290–295.
14. Rusnati, M., *et al.* (1997). Interaction of HIV-1 Tat protein with heparin. *J. Biol. Chem.* **272:** 11313–11320.
15. Tyagi, M., Rusnati, M., Presta, M., and Giacca, M. (2001). Internalization of HIV-1 Tat requires cell surface heparin sulfate proteoglycans. *J. Biol. Chem.* **276:** 3254–3261.
16. Leifert, J. A., Harkins, S., and Whitton, J. L. (2002). Full-length proteins attached to the HIV tat protein transduction domain are neither transduced between cells, nor exhibit enhanced immunogenicity. *Gene Ther.* **9:** 1422–1428.
17. Richard, J. P., *et al.* (2003). Cell penetrating peptides: a re-evaluation of the mechanism of cellular uptake. *J. Biol. Chem.* **278:** 585–590.
18. Seisenberger, G., Ried, M. U., Endreß, T., Büning, H., Hallek, M., and Bräuchle, C. (2001). Real-time single-molecule imaging of the infection pathway of an adeno-associated virus. *J. Biol. Chem.* **294:** 1929–1932.
19. Pelkmans, L., Kartenbeck, J., and Helenius, A. (2001). Caveolar endocytosis of simian virus SV40 reveals a new two-step vesicular-transport pathway to the ER. *Nat. Cell Biol.* **3:** 473–483.
20. Stehle, T., Yan, Y., Benjamin, T. L., and Harrison, S. C. (1994). Structure of murine polyomavirus complexed with an oligosaccharide receptor fragment. *Nature* **369:** 160–163.
21. Marjomaki, V., *et al.* (2002). Internalization of echovirus 1 in caveolae. *J. Virol.* **76:** 1856–1865.
22. Ikonen, E., and Parton, R. G. (2000). Caveolins and cellular cholesterol balance. *Traffic* **1:** 212–217.
23. Campbell, S. M., Crowe, S. M., and Mak, J. (2001). Lipid rafts and HIV-1: from viral entry to assembly of progeny virions. *J. Clin. Virol.* **22:** 217–227.
24. Montesano, R., Roth, J., Robert, A., and Orci, L. (1982). Non-coated membrane invaginations are involved in binding and invagination of cholera and tetanus toxins. *Nature* **296:** 651–653.
25. Nichols, B. J., *et al.* (2001). Rapid cycling of lipid rafts between the cell surface and Golgi complex. *J. Cell Biol.* **153:** 529–541.
26. Mundy, D., Machleidt, T., Ying, Y., Anderson, R. G., and Bloom, G. S. (2002). Dual control of caveolar membrane traffic by microtubules and the actin cytoskeleton. *J. Cell Sci.* **115:** 4327–4339.
27. Thomsen, P., Roepstorff, K., Stahlhut, M., and van Deurs, B. (2002). Caveolae are highly immobile plasma membrane microdomains, which are not involved in constitutive endocytic trafficking. *Mol. Biol. Cell* **13:** 238–250.
28. Lippincot-Schwartz, J., and Smith, C. L. (1997). Insights into secretory and endocytic membrane traffic using green fluorescent protein chimeras. *Curr. Opin. Neurobiol.* **7:** 631–6639.
29. Sieczkarski, S. B., and Whittaker, G. R. (2002). Dissecting virus entry via endocytosis. *J. Gen. Virol.* **83:** 1535–1545.
30. Marzio, G., Tyagi, M., Gutierrez, M. I., and Giacca, M. (1998). HIV-1 tat transactivator recruits p300 and CREB-binding protein histone acetyltransferases to the viral promoter. *Proc. Natl. Acad. Sci. USA* **23:** 13519–13524.
31. De Marchi, F., d'Adda di Fagagna, F., Falaschi, A., and Giacca, M. (1996). Activation of transcription factor NF-kappaB by the Tat protein of human immunodeficiency virus type 1. *J. Virol.* **70:** 4427–4437.
32. Caron, N. J., *et al.* (2001). Intracellular delivery of a Tat–eGFP fusion protein into muscle cells. *Mol. Ther.* **3:** 310–318.
33. Wachter, R. N., and Remington, S. J. (1999). Sensitivity of the yellow variant of green fluorescent protein to halides and nitrate. *Curr. Biol.* **9:** R628–629.
34. Cinelli, R., Ferrari, A., Pellegrini, V., Tyagi, M., Giacca, M., and Beltram, F. (2000). The enhanced green fluorescent protein as a tool for the analysis of protein dynamics and localization: local fluorescence study at the single-molecule level. *Photochem. Photobiol.* **71:** 771–775.
35. Wacher, I., Kaether, C., Kromer, A., Migala, A., Almers, W., and Gerders, H-H. (1997). Microtubule-dependent transport of secretory vesicles visualized in real time with a GFP-tagged secretory protein. *J. Cell Sci.* **110:** 1453–1463.
36. Fujimoto, T., Miyawaki, A., and Mikoshiba, K. (1995). Inositol 1,4,5-triphosphate receptor-like protein in plasmalemmal caveolae is linked to actin filaments. *J. Cell Sci.* **108:** 7–15.
37. van Deurs, B., von Bulow, F., Vilhardt, F., Holm, P. K., and Sandvig, K. (1996). Destabilization of plasma membrane structure by prevention of actin polymerization. Microtubule-dependent tubulation of the plasma membrane. *J. Cell Sci.* **109:** 1655–1665.
38. Frankel, A. D., and Pabo, C. O. (1988). Cellular uptake of the Tat protein from human immunodeficiency virus. *Cell* **55:** 1189–1193.
39. Mann, D. A., and Frankel, A. D. (1991). Endocytosis and targeting of exogenous HIV-1 Tat protein. *EMBO J.* **10:** 1733–1739.

doi:10.1016/S1525-0016(03)00122-9

40. Fang, B., Xu, B., Koch, P., and Roth, J. A. (1998). Intercellular trafficking of VP22–GFP fusion proteins is not observed in cultured mammalian cells. *Gene Ther.* **5:** 1420–1424.

41. Pelkmans, L., and Helenius, A. (2002). Endocytosis via caveolae. *Traffic* **3:** 311–320.

42. Pelkmans, L., Püntener, D., and Helenius, A. (2002). Local actin polymerization and dynamin recruitment in SV40-induced internalization of caveolae. *Science* **296:** 535–539.

43. Fittipaldi, A., *et al.* (2003). Cell membrane lipid rafts mediate caveolar endocytosis of HIV-1 Tat fusion proteins. *J. Biol. Chem.*, in press.

44. Cheng, F., Mani, K., van den Born, J., Ding, K., Belting, M., and Fransson, L. (2002). Nitric oxide-dependent processing of heparin sulfates in recycling S-nitrosylated glypican-1 takes place in caveolin-1-containing endosomes. *J. Biol. Chem.* **277:** 44431–44439.

45. Tumova, S., Woods, A., and Couchman, J. R. (2000). Heparan sulfate proteoglycans on the cell surface: versatile coordinators of cellular functions. *Int. J. Biochem. Cell Biol.* **32:** 269–288.

46. Eguchi, A., *et al.* (2001). Protein transduction domain of HIV-1 Tat protein promotes efficient delivery of DNA into mammalian cells. *J. Biol. Chem.* **276:** 26204–26210.

47. Bonifaci, N., Sitia, R., and Rubartelli, A. (1995). Nuclear translocation of an exogenous fusion protein containing HIV Tat requires unfolding. *AIDS* **9:** 995–1000.

48. Bender, F., Montoya, M., Monardes, V., Leyton, L., and Quest, A. F. (2002). Caveolae and caveolae-like membrane domains in cellular signaling and disease: identification of downstream targets for the tumor suppressor protein caveolin-1. *Biol. Res.* **35:** 151–167.